ELSEVIER

Fusion Engineering and Design 63–64 (2002) 597–608

Fusion Engineering and Design

www.elsevier.com/locate/fusengdes

# Dynamic chamber armor behavior in IFE and MFE

A.R. Raffray [a,*], G. Federici [b], A. Hassanein [c], D. Haynes [d]

[a] University of California, San Diego, 458 EBU-II, La Jolla, CA 92093-0417, USA
[b] ITER Garching Joint Work Site, Boltzmannstr. 2, 85748 Garching, Germany
[c] Argonne National Laboratory, 9700 South Cass Avenue, Argonne, IL 60439, USA
[d] Fusion Technology Institute, University of Wisconsin, 1500 Eng. Dr., Madison, WI 53706-1687, USA

**Abstract**

The chamber wall armor is subject to demanding conditions in both inertial fusion energy (IFE) and magnetic fusion energy (MFE) chambers. This paper assesses the requirements on armor imposed by the operating conditions in IFE and MFE, including energy deposition density, time of deposition and frequencies, and discusses their impact on the performance of the candidate armor materials.


*Keywords:* Magnetic fusion energy; Inertial fusion energy; Armor materials

## 1. Introduction

Inertial fusion energy (IFE) operation is cyclic in nature and the armor must accommodate the cyclic energy deposition while providing the required lifetime. Magnetic fusion energy (MFE) targets steady state operation and the armor needs to accommodate the steady state design heat fluxes. However, MFE operation also includes a number of dynamic operation scenarios (e.g. edge localized modes (ELMs), disruptions, runaway electrons and vertical displacement events (VDEs)) whose loading conditions must also be accommodated by the armor and where some commonality with IFE operation might exist.

The armor requirements of integrity, lifetime and compatibility with reactor operation are thus quite demanding for both MFE and IFE. Candidate armor materials are selected on the basis of these requirements. In IFE, the armor configuration includes both solid and liquid walls, the latter providing the possibility of armor replenishment prior to each shot. In MFE, although some attention has recently been given to liquid armor [1], solid armor remains the main candidate on which the R&D is focused [2]. In line with this MFE emphasis and with the intent of finding the widest armor commonality between MFE and IFE, this paper focuses on solid armor.

In MFE, the ITER design representing an example of the next-step reactor considers beryllium, tungsten and carbon as armor material for its plasma-facing components; however, beryllium would provide limited possibilities for further application to power plant reactor because of its

* Corresponding author. Tel.: +1-858-534-9720; fax: +1-858-534-7716
*E-mail address:* raffray@fusion.ucsd.edu (A.R. Raffray).

0920-3796/02/$ - see front matter 
PII: S0920-3796(02)00138-2

low melting point and operating temperature limit, and high sputtering yield [3]. Tungsten and carbon which provide high temperature accommodation are also considered as armor for IFE. This paper aims to assess the requirements on armor imposed by the operating conditions in IFE and MFE, including energy deposition density, time of deposition and frequencies, and to discuss their impact on the performance of the candidate armor materials. A particular focus of the paper is to ascertain the common issues and operating conditions between IFE and MFE with the goal of maximizing the synergy between chamber wall armor design and R&D for MFE and IFE.

## 2. Operating conditions

### 2.1. MFE armor operating conditions

MFE plasma-facing components (PFCs) must be designed to accommodate the steady state conditions and a number of off-normal conditions. PFCs include the first wall, baffle, limiter and divertor of which the divertor would typically face the more demanding loads and operating conditions. For example, the ITER divertor must accommodate a peak steady state heat flux of $\sim$ 10 MW/m$^2$ and peak particle flux of $\sim 10^{24}$/m$^2$ s. The divertor must also accommodate a number of dynamic operation scenarios, namely ELM scenarios and disruptions. The ITER divertor conditions associated with these scenarios are summarized in Table 1.

### 2.2. IFE Armor operating conditions

The chamber wall armor faces demanding conditions in IFE chambers. IFE operation is cyclic in nature ($\sim$1 to 10 Hz) and consists of injection of a target on which is focused the driver (laser or heavy ion beam) to create the micro-explosion. Following each micro-explosion, the chamber wall is subjected to a large flux of photons, energetic particles and neutrons. Depending on the chamber wall loads, a background gas may be needed to attenuate the energy deposition on the chamber wall by absorption and re-radiation over a longer time.

Example conditions associated with IFE are shown in Table 1 for a laser-driven direct-drive target with a yield per shot of 154 MJ and corresponding neutron, fast ion, debris ion and photon energy partition of 71, 13, 16, and 1%, respectively [4]. The corresponding photon, fast ion and debris ion spectra are shown in Figs. 1–3, respectively. A higher yield direct-drive target ($\sim$ 400 MJ) has also been proposed with about the same energy partitioning among ions and photons [4].

Another target option, known as the indirect-drive target, utilizes a radiation hohlraum enclosure in which sits the D-T target pellet. Such an option has been considered in particular in conjunction with a heavy ion beam driver. The resulting photon and ion energy partitioning and fluxes are much more challenging for a dry wall configuration necessitating a substantial amount of protective chamber gas for wall survival. For example, for the heavy ion beam indirect-drive target of Ref. [4], the energy partition among neutron, fast ion, debris ion and photon is 69, 2, 4, and 25%, respectively. Much more energy is carried by the photon whose spectrum is also softer, as shown in Fig. 1.

Although the base operating conditions of IFE and MFE are fundamentally different, an interesting parallel can be drawn between IFE and MFE armor conditions for some cases. For example, as shown in Table 1, the maximum particle flux and the Type 1 ELMs energy density and frequency for the ITER divertor are within about one order of magnitude of those for IFE. This provides the possibility of cross-fertilization and synergy when planning and carrying out supporting R&D.

## 3. Armor

Issues driving the choice of armor material tend to be similar for MFE and IFE and can be broadly classified as follows:

1) High temperature and thermal stress accommodation.

Table 1
Conditions assumed for ITER ELMs, VDEs and disruptions compared to conditions associated with a typical direct-drive target IFE (NRL154MJ target)

| | ITER Type-I ELMs | ITER VDEs | ITER disruption thermal quench | Typical IFE operation (direct-drive NRL target) |
|---|---|---|---|---|
| Energy | 10–12 MJ | $\sim 50$ MJ/m$^2$ | 100–350 MJ | $\sim 0.1$ MJ/m$^2$ |
| Affected area | 5–10 m$^{2a}$ | A few m$^{2a}$ | $\sim 10$ m$^{2a}$ | Chamber wall ($R \sim 5$–10 m) |
| Location | Near divertor strike points | Surface/bulk | Near divertor strike points | Bulk($\sim$ μm's) |
| Time | $\geqslant 200$ μs | $\sim 0.3$ s | $\sim 1$ ms | $\sim 1.3$ μs |
| Max. temperature | Melting point/sublimation temperature | Melting point/sublimation temperature | Melting point/sublimation temperature | $\sim 2000$–3400 °C(for dry wall) |
| Frequency | Few Hz | $\sim 1/100$ cycles | $\sim 1/10$ cycles | $\sim 10$ Hz |
| Base temperature | $\geqslant 500$ °C | $\sim 200$ °C | 200–1000 °C | $\sim > 700$ °C |
| Particle fluxes | $10^{24}$ /m$^2$ s(peak under normal operation) | | | $\sim 10^{23}$ m$^2$ s |

[a] Large uncertainties exist.

2) Erosion which limits the armor lifetime. In addition, erosion in the case of MFE can create a source of impurities, which cool and dilute the plasma. In the case of IFE ablated material must be considered in the chamber clearing process to ensure that after each shot the chamber returns to a quiescent state in preparation for the target injection and the firing of the driver for the subsequent shot.
3) Tritium inventory due to tritium implantation and trapping in the bulk of the material and, for carbon only, to co-deposition with eroded carbon redeposited in cold areas.

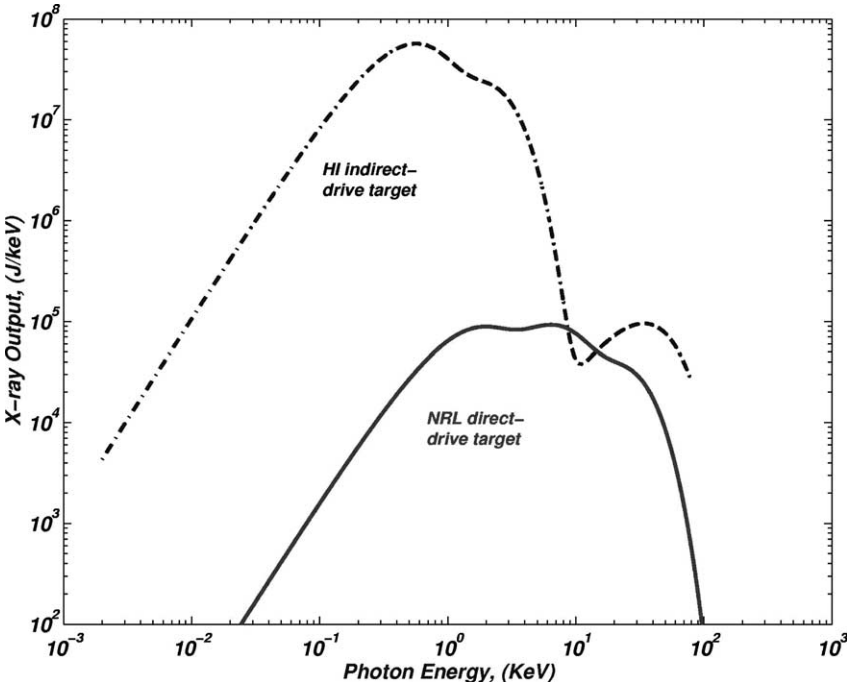


Fig. 1. Photon spectra from NRL154 MJ direct-drive target and heavy ion beam indirect-drive target [4].

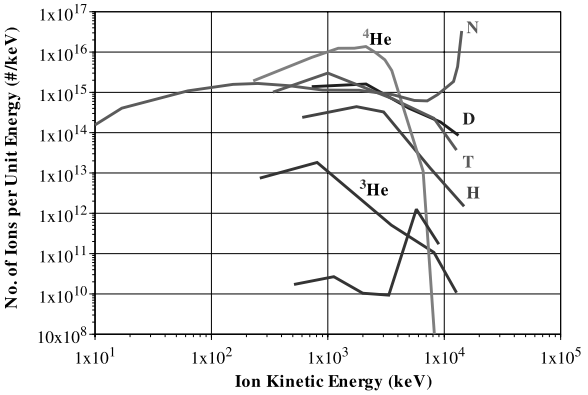


Fig. 2. Fast ion spectra from NRL154 MJ direct-drive target [4].

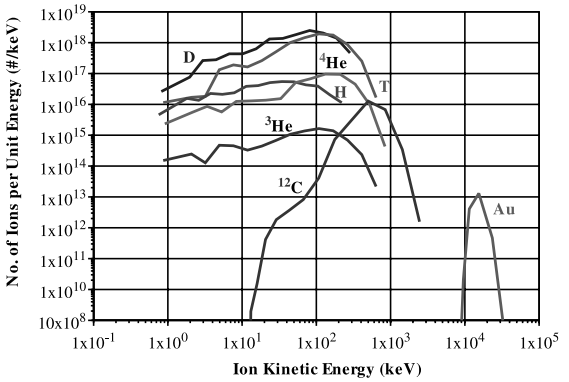


Fig. 3. Debris ion spectra from NRL154 MJ direct-drive target [4].

In addition to these issues, several other considerations, such as chemical compatibility and activation, come into play when evolving the choice of armor configuration and material. Carbon which shows good high-temperature resistance and thermal properties is a candidate armor. However, several mass loss processes have been identified in carbon including chemical erosion and radiation enhanced sublimation which lead to key concerns of lifetime and tritium inventory through co-deposition, as will be discussed in the next section. Refractory metals, such as tungsten, are attractive candidates since they also have good high temperature capability without the tritium co-deposition and inventory concern. However, melting can be an issue for severe energy deposition scenarios depending on the stability of the melt layer and on the form of the resolidified material. Both carbon and tungsten are currently considered as armor material candidates for MFE and IFE. In addition, ITER considers beryllium as PFC armor for its moderately loaded first wall. However, because of its low melting point and high sputtering yield, it would not be compatible with the high temperature and lifetime requirements of commercial reactor operation.

### 3.1. Armor behavior under MFE operation

In MFE devices the interaction of the edge plasma with the PFCs is determined by plasma density, temperature, flows, power fluxes, and neutral fluxes, and is most intense in the vicinity of the 'strike point' where the separatrix intersects the divertor target plate. These, in turn, determine the rate of physical sputtering, chemical sputtering, ion implantation, and impurity generation. Neutral fluxes also cause erosion and co-deposition, even on areas not contacted by the plasma, e.g., the main chamber wall. Plasma ions approaching the material surfaces are accelerated by the sheath potential to an energy $E_0 \approx 2T_t + 3ZT_t$, where $T_t$ is the plasma temperature adjacent to the target plate and $Z$ is the charge of the ion. Above a certain threshold, the exchange of kinetic energy between the impacting ions and atoms in the top monolayers of the material, can knock surface atoms out into the plasma in a process termed physical sputtering.

For carbon, chemical reactions with incident hydrogen ions are also possible, leading to the formation of volatile hydrocarbon molecules or to loosely bound hydrocarbon precursors, which can be sputtered with much lower threshold energy. Chemical erosion is a complicated multi-step process that depends on particle energy and flux, surface temperature and material properties such as crystalline structure, and may be influenced by impurity atoms in the lattice. Another erosion process observed with carbon is radiation enhanced sublimation which increases with temperature in the range of about 1200–2000 K and is hypothesized to result from the sublimation of radiation-induced interstitials.

In addition to erosion that occurs during the quiescent phase of the discharge, erosion during ELMs which produce a periodic very rapid expulsion of thermal energy and particles from the edge region into the scrape-off layer and finally to the surfaces of the divertor and off-normal events (e.g. disruptions, vertical displacement events, and runaway electrons) represents a major concern for component survivability and lifetime. These events are anticipated to cause surface damage and high erosion losses due to surface vaporization, cracking and spallation, and melt-layer loss. Besides surface damage effects, plasma instabilities of longer duration such as vertical displacement events, or those that deposit energy more deeply (e.g. runaway electrons) can produce significant bulk effects. These include large temperature increases in the armor and heat-sink/structural materials and at their interface, causing high thermal stresses, possible structure melting, and material fatigue and failure and high heat flux levels in coolant tubes. The result may be burnout of the tubes, leading to significant down times for repair and maintenance. Finally, the production, transport and re-deposition of the eroded materials from vaporization, melt-layer splashing, and macroscopic particle emission are of major concern for plasma contamination, and for safety (dust hazard). The relevant plasma-material interactions in MFE are comprehensively reviewed in Ref. [5].

Divertor plate erosion during Type I ELMs and disruptions challenges the design of the ITER divertor [6]. To avoid the erosion and tritium concerns linked with carbon it is desirable to utilize W over the whole divertor surface including the strike point. However, the lifetime of a W target near the strike points remain uncertain due to the loss of the melt layer (and the properties of the resolidified material) that develops under disruptions and Type I ELMs. Operational regime free of Type I ELMs, which are compatible with required confinement (e.g. Type II ELMs), and minimisation of disruptions to be accrued by operating experience in ITER together with availability of disruption mitigation techniques (to be developed and tested in existing tokamaks), would substantially improve prospect for early installation of tungsten in the ITER divertor.

The consequences of transient heating events (i.e. ELMs and disruptions) in a next-step tokamak has been more clearly illuminated by the development of complex two- and three-dimensional simulations. The predictive abilities of these codes is somewhat uncertain since no tokamak benchmark experiments are available (current devices do not have the necessary energy density). Nevertheless, the predicted magnitude of PFC damage by melting and evaporation has alerted the fusion research community to the urgent need to control or eliminate these transient events in the next-step tokamak. Work is in progress to test effective disruption mitigation techniques and to find operational regime, with good plasma confinement that free of Type I ELMs. Example results of transient temperature response and erosion calculations are shown below for different armor materials during type I ELMs and disruption, whose loading conditions are specified in Ref. Table 1.

### 3.1.1. ELMs

The RACLETTE code described in Refs. [7,8] is presently used to predict ELM erosion for ITER. It includes all the key surface heat transfer processes such as evaporation, melting, and radiation, and their interaction with the PFC block thermal response and the coolant behavior. It is based on an implicit finite difference scheme, which allows for temperature-dependent material properties, with the energy balance equations at the surface, providing boundary conditions for the solution.

Fig. 4 and Fig. 5 show the time evolution of the surface temperature for CFC and W, respectively, together with the corresponding melt-layer thickness (for W) and vaporized thickness following a Type I ELM (1 MJ/m$^2$, 0.2 ms [6]). The calculations were done with the RACLETTE code neglecting any vapor shielding effect which is expected to increase at higher energy densities. An initial heat flux of 10 MW/m$^2$ is assumed and determines the steady-state temperature distribution. The maximum surface temperature is $\sim$ 4000 °C for CFC and $\sim$5000 °C for W, and

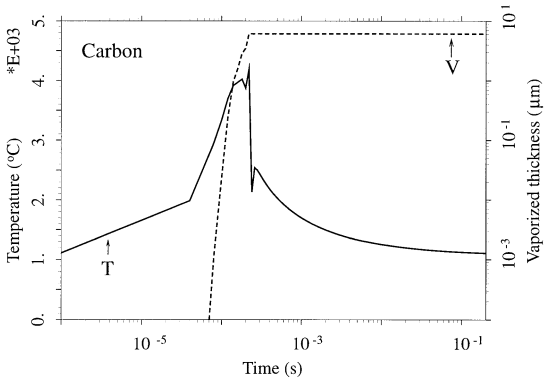


Fig. 4. Time evolution of surface temperature for CFC and vaporized thickness following a Type I ELM (1 MJ/m$^2$, 0.2 ms) assuming an initial steady state condition with a heat flux of 10 MW/m$^2$, calculated by the RACLETTE code [7,8].

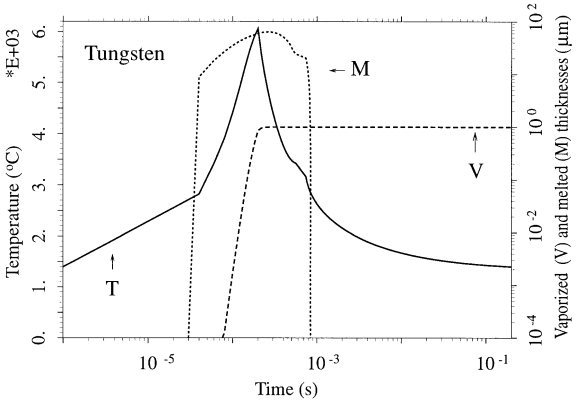


Fig. 5. Time evolution of surface temperature for W and melt layer and vaporized thicknesses following a Type I ELM (1 MJ/m$^2$, 0.2 ms) assuming an initial steady state condition with a heat flux of 10 MW/m$^2$, calculated by the RACLETTE code [7,8].

the temperature drops to the initial value in about 10 ms. Thus, for ELM frequencies of the order of 1–2 Hz, no temperature ratcheting effects are expected and the results of analysis of a single ELM can be extrapolated to a larger number of ELMs.

The evaporated CFC thickness is $\sim 5$ μm, corresponding to $\sim 20$ mm of material loss per hour for a frequency of 1 Hz. Thus, a large number of ELMs with energy densities $> 1$ MJ/m$^2$ cannot be tolerated in ITER. The evaporated thickness in the case of W is lower ($\sim 1$ μm per event). However, the melt-layer thickness is $\sim 70$ μm and a key lifetime issue would be the stability of the melt layer and the corresponding fractional loss of melted material.

### 3.1.2. Disruptions

Surface vaporization losses from metallic plasma-facing materials are generally small (only a few microns) over a wide range of plasma conditions during short (i.e. $\ll 1$ s) plasma instabilities. The thickness of the melt layer on metallic components can be one to two orders of magnitude higher than surface vaporization losses. This is illustrated in Fig. 6 (taken from Ref. [9]) that shows the time evolution of a tungsten surface temperature, melt-layer thickness), and vaporization losses during a disruption for an incident plasma energy of 10 MJ/m$^2$ deposited in a disruption time of 1 ms as predicted by the A*THERMAL-S code (part of the HEIGHTS package) [10]. An initial magnetic field strength of $5T$ with an incident angle of $2^\circ$ is used in this calculation. The sharp initial rise in surface temperature is due to the direct energy deposition of incident plasma particles at the material's surface. The subsequent decrease in the surface temperature is caused by the reduction in absorbed heat flux due to the vapor shield and conduction of heat into the material. The subsequent behavior is mainly determined by the energy flux from the emitted photon radiation in the vapor cloud, as

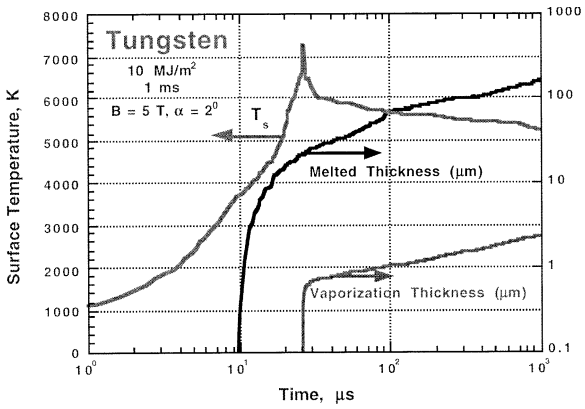


Fig. 6. Time evolution of tungsten surface temperature, melt layer, and eroded thickness following a plasma disruption predicted by the A*THERMAL-S CODE [9].

discussed above, and by vapor-electron heat conduction. Again, a key lifetime issue is the frequency of such disruption energy deposition at a given location and the W melt-layer behavior.

In contrast to the divertor, the erosion rate at the wall during normal operation is low enough that the PFCs do not need replacement; however, the total amount of eroded material may be significant because of the larger area. This material will most likely go to the divertor where it will affect the composition and performance of the divertor surface and contribute to tritium co-deposition. Results of analysis done to compute erosion of the first-wall (due to fuel charge-exchange neutrals and ions and impurity ions) and the subsequent transport of material on the divertor surfaces are presented in Ref. [3].

### 3.2. Armor behavior under IFE operation

Several forms of protection for the surviving target chamber structures have been proposed for IFE reactors. The structures must be protected from the highly cyclic nature of the thermal loading from high energy photons and ions and satisfy the constraint that target chamber conditions are re-established before the next target injection. Until recently, all of the main line IFE chamber designs relied on a gas medium which absorbs the target x-rays and ions and re-emits the energy over a time scale sufficiently long that the permanent target chamber structures can cope with the insult. Re-emission of the absorbed energy occurs through one of two processes. Photons from the relaxation of excited electrons through Bremsstrahlung, radiative recombination or photo-de-excitation are emitted at rates determined by the emission opacity of the gas. Some of the absorbed energy is thermalized, and the gas conducts the heat to the wall through conduction. The effect of these processes is to stretch the time scales associated with the insult to the wall and to mitigate the resulting heat flux. In all cases, the effects of the chamber gas on driver beam propagation, target injection, target heating must also be considered.

In addition, the thermal loads on the wall due to photons and ions of different energies would occur at different times due to the time of flight spreading effect. Typically photons would reach the wall within about 10 ns whereas most ions would reach the wall between $\sim 0.1$ and 3 μs depending on their energies. This would also mitigate the insult to the first wall, affording an opportunity to reduce the chamber radius, to increase the first wall operating temperature, or to minimize or remove the need for a buffer gas [11].

In this section, example calculations for chamber wall survival are presented for tungsten and carbon armor materials. Fig. 7 shows the tungsten temperature history in the absence of a protective gas calculated from a one-dimensional model based on RACLETTE [7,8]. These calculations were done for energy deposition values corresponding to the 154 MJ direct-drive target photon and ion spectra shown in Figs. 1–3 [11]. An attenuation calculation was used for the photon energy deposition based on data for the attenuation coefficient in the material (including photo-electric and Compton scattering effects) as a function of the photon energy [12]. The ion deposition calculation included both the electronic and nuclear stopping powers which were obtained as a function of ion energy from SRIM [13].

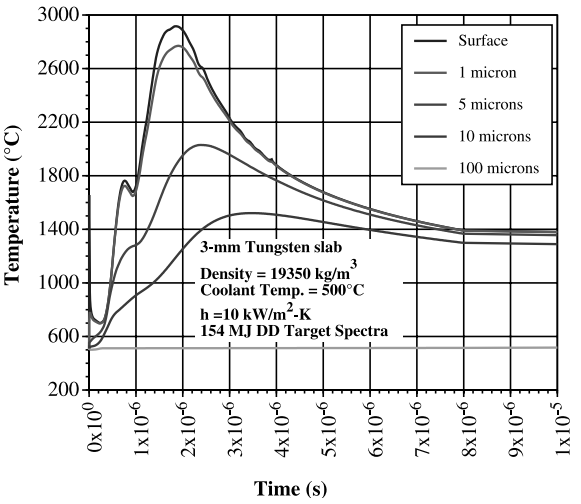


Fig. 7. Temperature history of tungsten armor under 154 MJ direct-drive target spectra threat without protective chamber gas.

From the W results shown in the figure, the photon energy deposition is very fast and creates an instantaneous temperature increase of about 1150 °C. The maximum W temperature is < 3000 °C. If the melting point (3410 °C) is considered as a limit, this would provide some margin for adjustment of parameters such as target yield, chamber size, coolant temperature and protective gas pressure. Another interesting observation is that significant temperature changes occur in a very thin region of the armor ( < 100 μm). On this basis, a design with separate functions is preferred: a thin armor providing the high energy accommodation function bonded to a structural substrate providing the structural function and interfacing with the blanket which effectively see quasi steady-state conditions. Calculations for C under the 154 MJ direct-drive target threat spectra showed a maximum temperature of < 2000 °C with an associated annual sublimation loss of less than 1 μm, providing even more margin to allow for design optimization on various parameters.

Similar calculations were done for the 400 MJ direct-drive target. The resulting temperatures for both C and W are unacceptable for a case without protective gas. However, when comparing the W results with those shown in Fig. 6 for the MFE disruption case it is interesting to see that the maximum temperature ( ~ 7000 °C) and corresponding melt layer ( ~ 10 μm) are of the same order in both cases although the time to reach the maximum temperature differs ( ~ 2 μs for the IFE case and ~ 25 μs for the MFE case).

Calculations were also done for cases with protective gas using the one-dimensional Lagrangean radiative-hydrodynamics code BUCKY [14]. In this code, prompt X-ray deposition is modeled using cold opacities from Biggs and Lighthill. Deposition of ion energy is approximated by the theory of Melhorn [15], and the free electron contribution interpolates between the low energy Lindhard–Scharff limit and the high energy Bethe limit. Radiation transport is calculated here in the flux-limited multi-group diffusion approximation [16]. Energy that reaches the wall is treated as a source term in a thermal diffusion equation. As the temperature in a wall cell approaches the vaporization temperature, the zone begins to vaporize at a rate determined by the relative rates of vaporization and condensation, as determined by the kinetic theory of Labuntsov and Kryukov [17].

A key assumption in setting the armor lifetime is the allowable armor thickness ablation per shot. Ablation of less than one atomic monolayer is not physically possible and past studies, such as SOMBRERO [18], have assumed a criterion of a monolayer loss per shot which, for illustrative purposes, is also assumed in the example calculations shown below. It is recognized, however, that loss of even one atomic monolayer ( ~ 2 Å) per shot would result in unacceptably high annual armor erosion ( ~ cm's) and that a more severe constraint has to be set (e.g. assuming that so many atoms are lost per shot corresponding to a uniform average loss of a fraction of a monolayer).

As an example of the protective gas requirement to provide a desired chamber erosion lifetime, the chamber gas density required to maintain an assumed constraint of one monolayer of vaporized wall material per shot was estimated as a function the initial chamber armor temperature. Fig. 8 illustrates the results for a carbon armor for a chamber of radius of 6.5 m with xenon as protective gas. Results for two different threat

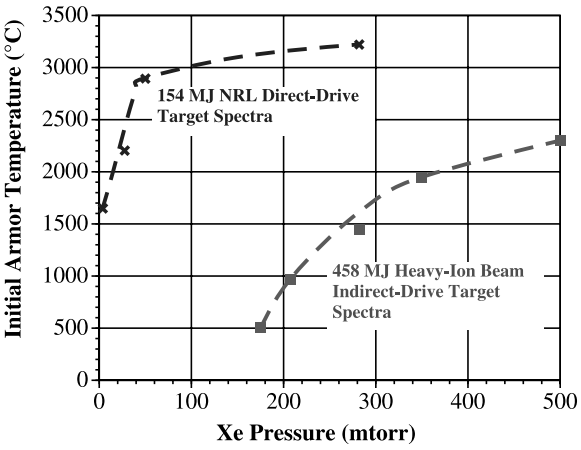


Fig. 8. Combination of carbon armor initial temperature and required Xe gas density expressed in Torr at ST (1 Torr = $3.54 \times 10^{16}$ particles/cm$^3$) for sublimation of one monolayer per shot. (Chamber wall radius = 6.5 m). Results for two different target threats are shown: a 154 MJ direct-drive target, and a 458 MJ closely coupled heavy ion beam indirect-drive target.

spectra are shown; the 154 MJ radiatively smoothed direct-drive target discussed in Section 2.1 and whose photon and ion spectra are shown in Figs. 1–3; and the 458 MJ closely coupled heavy ion beam indirect-drive target described in Section 2.1. Note that these BUCKY results tend to be conservative due to the relatively coarse binning of the target ion threat spectra used in the calculations and to some extent to the assumed sublimation model and data. These effects are under investigations.

The results indicate that for the 154 MJ target, the carbon armor would meet this erosion constraint without any protective gas if the initial armor temperature (set by the coolant temperature) is $\sim$1600 °C. For the indirect-drive case where most of the non-neutronic energy is emitted as soft X-rays, the buffer gas requirement is more demanding ($\sim$210 mTorr for an initial armor temperature of 1000 °C). Target injection and driver beam requirements must also be considered when setting the protective gas density. For example, direct-drive targets require high thermal control and heat transfer from the background gas during injection is limited. This would limit the gas pressure for direct-drive target and probably require larger chambers or lower coolant temperature for the higher yield case.

For the more massive and thermally shielded indirect-drive target, these constraints are much more relaxed and a higher background gas density would be acceptable. However, the effect on the driver needs to be considered such as laser breakdown in the case of a laser driver.

Similar calculations were done for tungsten with the goal of avoiding melting. Essentially the same observations about the required gas pressure can be made for the direct-drive case. However, for the indirect case, the large amount of energy carried by soft X-rays produces a very high surface heat flux on the tungsten resulting in unacceptable melting. Thus, tungsten is more suited for protecting the chamber wall from the threat posed by directly driven laser IFE targets where the absence of a hohlraum prevents the conversion of target ion debris energy into soft, potentially damaging, X-rays.

## 4. Key issues and R&D priority

Erosion of the armor over many pulses, and redeposition of eroded material (primarily carbon) in combination with tritium in cold areas of the machine represent critical issues for the design, operation, and safety of MFE and IFE systems. In addition, in MFE systems, erosion creates a source of impurities, which cool and dilute the plasma, while in IFE systems erosion must be considered when setting the chamber conditions prior to each shot for target injection and driver firing.

In MFE systems, deposition of material onto PFCs alters their surface composition and can lead to long term accumulation of large in-vessel tritium inventories. Retention and recycling of hydrogen from PFCs affects fuelling efficiency, plasma density control and the density of neutral hydrogen in the plasma boundary which impacts particle and energy transport. Many of the underlying physical processes such as sputtering, implantation, diffusion and trapping of hydrogen have been studied for many years and are fairly well understood. However, the development and validation of reliable models to simulate effects of plasma material interactions on MFE systems operation and make predictions for future machines is still in progress. Information on tritium inventory from co-deposition on cooler surfaces and on armor erosion mechanisms would be fully applicable for IFE also and represent R&D areas with the highest synergy potential.

Observations and dedicated experiments from current MFE devices illustrate the tritium inventory concern. Tritium fuel has been successfully used in the tokamak fusion test reactor (TFTR) and the joint european torus (JET) producing 10 and 16 MW of fusion power respectively [19,20]. A large fraction of tritium was retained during DT plasma operations in TFTR and JET by co-deposition with eroded carbon and by isotope exchange with previously retained deuterium [21,22]. When the tritium in-vessel inventory approached the administrative safety limit, it was removed by extensive campaigns involving several weeks of glow discharge cleaning and deuterium operation. An unexpectedly large amount of tritium was also transported to the JET sub-

divertor region. This operation experience pointed clearly to the problem associated with the formation of T-rich carbon co-deposited layers ($\geqslant 50$ μm) in cold areas during operations. The retention experience of Alcator C-mod [23] is particularly interesting in this respect since it is lined with Mo tiles and there are no carbon PFCs. The analysis showed that most of the D inventory was implanted (not co-deposited) on main chamber wall and that the fraction of D retained is drastically lower ($\sim 100$ times) than in other tokamaks with carbon PFCs. While tritium retention is not a significant limit to plasma operations in today's devices, the high rate of tritium retention and slow rate of tritium removal would be unacceptable in both a next-step device and in a fusion reactor where operations could be quickly terminated for fuel economy reasons [24], and because the total tritium in-vessel mobilizable inventory must be restricted to avoid the need for public evacuation under the worst possible accident. This would also apply to an IFE reactor.

Operation experience in today's tokamaks strongly indicates that both MFE and IFE devices with carbon armor will accumulate tritium by co-deposition with the eroded carbon in relatively cold areas (such as in penetration lines). Carbon is currently chosen in ITER to clad the divertor target near the strike points because of its greater resilience to excessive heat loads during ELMs and disruptions. However, maintaining carbon in the design has a strong impact on the control of the T-inventory, and efficient in-situ techniques are required to recover the tritium retained in the co-deposited layers to avoid frequent interruptions imposed by precautionary operating safety limits or necessitated by fuel economy. The number of plasma pulses before the inventory limit (e.g. less than 500 g of in-vessel co-deposited tritium in ITER) is reached is estimated to be only 70–170 pulses (Fig. 9). Although several alternatives are being considered for the removal of the T-rich co-deposited layers, their removal from a machine using significant quantities of carbon is a major unsolved problem. Certainly, this provides a strong motivation to consider other armor materials for MFE and IFE applications as this would

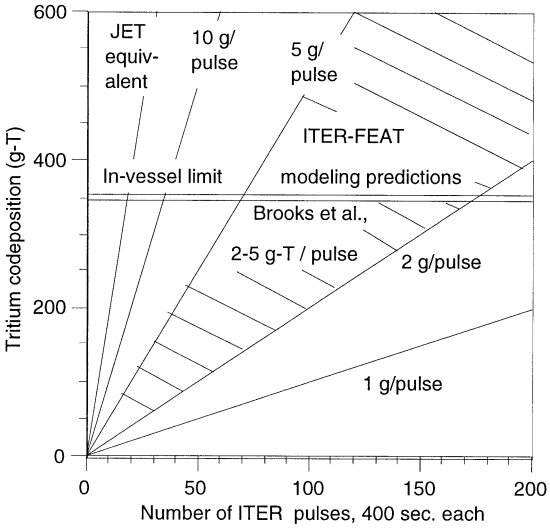


Fig. 9. Tritium retention for ITER, showing modeling predictions [25] and JET DTE equivalent rate. The inventory limit (shown by double line) is predicted to be reached in approximately 100 pulses.

render the control of tritium inventory much more manageable.

In addition to micro-level erosion processes such as vaporization and sputtering, macroscopic erosion phenomena can seriously decrease the lifetime of PFCs. These include melt-layer loss in the case of metallic armor and brittle destruction in the case of carbon armor.

During a reactor disruption, the melt layer formed on the surface of a metallic armor is subject to various forces such as electromagnetism, gravitation, mechanical vibration, plasma momentum, surface tension, and ablation recoil which can cause melt-layer loss [26]. Experimental observations in laboratory disruption simulation devices are consistent with two important mechanisms of melt-layer removal. These mechanisms are melt splashing due to the formation, growth, and explosion of vapor bubbles inside the liquid layer, and growth of hydrodynamic instabilities due to plasma impact momentum ('plasma wind') at the liquid surface and forces generated by current decay in the liquid metal layer. Therefore, hydrodynamic instabilities, such as the Kelvin–Helmholtz instability, will arise and form liquid droplets that will be carried away by the plasma wind. The

amount and rate of melt-layer loss is difficult to predict and is expected to depend on many parameters, such as heat flux, impurity and gas content, material properties, and disrupting plasma parameters. More work is needed to study the details of macroscopic erosion of metallic materials during an intense deposition of energy.

In carbon-based material (CBM), a phenomenon, called 'brittle destruction,' has been observed in various disruption simulation facilities [26]. Physical mechanisms that cause brittle destruction of CBMs are not yet clear. One mechanism could be cracking caused by thermo-mechanical stresses that develop during the intense deposition of energy. Another proposed mechanism is that material is ejected by the sharp rise in the pressure of gas trapped in the network of pores between intergranular and intercrystallite boundaries that can cause explosive ejection of material. These processes are likely to depend on the material microstructure. The macroscopic erosion of CBMs will depend on three main parameters: net power flux to the surface, exposure time, and the threshold energy required for brittle destruction. The required energy is critical in determining the net erosion rate of CBMs and is currently estimated from disruption simulation experiments. Additional experimental data and detailed modelling are required to evaluate the erosion of CBMs and in particular the role of brittle destruction.

Finally, R&D effort is also needed on the fabrication of the armor material on its bonding to a structural material, and on the armor and bond integrity under operation. In the case of IFE in particular concerns exist as to the applicability of material properties and behavior evolved under equilibrium or moderate transients to the highly cyclic conditions at the armor surface. In addition, the continuous bombardment of ions and their deposition in a shallow region near the armor surface raise concerns of weakening of the armor thermo-mechanical properties and possible macroscopic cracking and failure if the ions cannot diffuse back to the surface and to the chamber. This could be the case for He which has very low diffusion in tungsten for example and where effort is needed to address the issue and find solutions such as the possible use of a porous nanostructure through which the He could diffuse back to the chamber.

## 5. Conclusions

The chamber wall armor is subject to demanding conditions in both IFE and MFE chambers. IFE operation is cyclic in nature while MFE operation targets steady state. However, there are a number of off-normal MFE operation scenarios in particular for the next-step device whose loading conditions on the armor show some commonality with IFE. This is particularly relevant for ELMs scenarios whose energy density and frequency are within an order of magnitude of IFE operation.

The armor requirements of integrity, lifetime and compatibility with reactor operation are quite demanding for both MFE and IFE in view of the challenging operating conditions both in term of incident heat fluxes and particle fluxes. Carbon has been considered as armor material for both MFE and IFE dry wall systems. However, a major concern for the design, operation, and safety of MFE and IFE systems is the erosion of the carbon armor over many pulses, and distribution of eroded material in combination with tritium. This provides a strong motivation for evolving performing armor materials other than carbon. Refractory metals, such as tungsten, are increasingly considered for MFE application and have been recently considered for IFE operation also. They provide high temperature capability without the major tritium inventory concern. However, melting is an issue for high energy deposition and the stability of the melt layer and integrity of the resolidified material must be addressed. As part of the R&D need to understand erosion, lifetime and tritium behavior associated with the armor, a key aspect is the characterization of properties and parameters normally evolved under equilibrium (or slow transient) conditions to dynamic conditions in particular for the highly-pulsed, irradiated IFE conditions.

This interest from the MFE and IFE communities on similar armor materials and related issues

provide a fertile ground for maximizing the synergy between MFE and IFE armor R&D.

## References


[1] The APEX Team, M.A. Abdou, Fus. Eng. Des. 54 (2001) 181–247.
[2] G. Federici, et al., Selection of Plasma-Facing Materials in Next-Step Fusion Devices, 19th Symposium on Fusion Engineering, SOFE, January 22–25, (2002), Atlantic City, New Jersey.
[3] G. Federici, et al., Erosion of Plasma-Facing Components in ITER, to be presented at ISFNT-6, San Diego, CA, April (2002).
[4] Available at http://aries.ucsd.edu/ARIES/WDOCS/ARIES-IFE/SPECTRA/
[5] G. Federici, C.H. Skinner, et al., Nucl. Fusion 41 (2001) 1967.
[6] A. Loarte, et al., Proceeding of the 18th International Conference Sorrento, 2000, IAEA, Vienna (2001) IAEA-CN-77. CD-ROM file ITERP/11(R), and http://www.iaea.org/programmes/ripc/physics/fec2000/html/node245.htm#55022
[7] A.R. Raffray, G. Federici, RACLETTE: a model for evaluating the thermal response of plasma facing components to slow high power plasma transients—Part I: theory and description of model capabilities, J. Nucl. Mater. 244 (1997) 85–100.
[8] G. Federici, A.R. Raffray, RACLETTE: a model for evaluating the thermal response of plasma facing components to slow high power plasma transients—Part II: analysis of ITER plasma facing components, J. Nucl. Mater. 244 (1997) 101–130.
[9] A. Hassanein, et al., J. Nucl. Mater. 241–243 (1997) 288.
[10] A. Hassanein, I. Konkashbaev, J. Nucl. Mater. 273 (1999) 326.
[11] A.R. Raffray, et al., Assessment of IFE Dry Chamber Wall, Fusion Eng. Des., (in press).
[12] Available at http://aries.ucsd.edu/LIB/PROPS/PHOTON/
[13] Available at http://www.srim.org/
[14] R.R. Peterson, et al., Fusion Tech. 30 (1996) 783.
[15] Melhorn, J. Appl. Phys. 52 (1981) 6522.
[16] J.J. MacFarlane, P. Wang, Phys. Fluids B 3 (1991) 3494.
[17] Labuntsov, Kryukov, Int. J. Heat Mass Transfer 22 (1979) 989.
[18] I.N. Sviatoslavsky, et al., Fusion Tech. 21 (1992) 1470.
[19] A. Gibson, et al., Phys. Plasmas 5 (1998) 1839.
[20] R.J. Hawryluk, Rev. Modern Phys. 70 (1988) 537–587.
[21] C.H. Skinner, et al., J. Nucl. Mater. 290–293 (2001) 486.
[22] P. Andrew, et al., Fusion Eng. Des. 47 (1999) 233.
[23] W.R. Wampler, et. Al., Long-term Retention of Deuterium and Tritium in Alcator C-Mod, in Proceeding of the 18th IEEE/NPSS Symposium. Fus. Eng., (1999) 267.
[24] G. Federici, et al., J. Nucl. Mat. 266-269 (1999) 14.
[25] G. Federici, et al., Phys. Scripta T91 (2001) 76.
[26] A. Hassanein, 'Prediction of Material Erosion and Lifetime during Major Plasma Instabilities in Tokamak Devices,' review-article, Fusion Eng. Design, (in press).